PASJ: Publ. Astron. Soc. Japan , 1–??,

Peculiarly Narrow SED of GRB 090926B with MAXI and Fermi/GBM

Motoko Serino,[1] Atsumasa Yoshida,[2] Nobuyuki Kawai,[3] Yujin E. Nakagawa,[4] Tatehiro Mihara,[1] Yoshihiro Ueda[5] Satoshi Nakahira,[1] Satoshi Eguchi,[5] Kazuo Hiroi,[5] Masaki Ishikawa,[6] Naoki Isobe,[7] Masashi Kimura,[8] Hiroki Kitayama,[8] Mitsuhiro Kohama,[9] Takanori Matsumura,[10] Masaru Matsuoka,[1,9] Mikio Morii,[3] Motoki Nakajima,[11] Hitoshi Negoro,[12] Megumi Shidatsu,[5] Tetsuya Sootome,[1] Kousuke Sugimori,[3] Mutsumi Sugizaki,[1] Fumitoshi Suwa,[12] Takahiro Toizumi,[3] Hiroshi Tomida,[9] Yohko Tsuboi,[10] Hiroshi Tsunemi,[8] Shiro Ueno,[9] Ryuichi Usui,[3] Takayuki Yamamoto,[1] Kazutaka Yamaoka,[2] Makoto Yamauchi,[13] Kyohei Yamazaki,[10] and the MAXI team

[1]*MAXI team, Institute of Physical and Chemical Research (RIKEN), 2-1 Hirosawa, Wako, Saitama 351-0198*
motoko@crab.riken.jp

[2]*Department of Physics and Mathematics, Aoyama Gakuin University, 5-10-1 Fuchinobe, Chuo-ku, Sagamihara, Kanagawa 252-5258*

[3]*Department of Physics, Tokyo Institute of Technology, 2-12-1 Ookayama, Meguro-ku, Tokyo 152-8551*

[4]*Research Institute for Science and Engineering, Waseda University, 17 Kikui-cho, Shinjuku-ku, Tokyo 162-0044*

[5]*Department of Astronomy, Kyoto University, Oiwake-cho, Sakyo-ku, Kyoto 606-8502*

[6]*School of Physical Science, Space and Astronautical Science, The graduate University for Advanced Studies (Sokendai), Yoshinodai 3-1-1, Chuo-ku, Sagamihara, Kanagawa 252-5210*

[7]*Institute of Space and Astronautical Science(ISAS), Japan Aerospace Exploration Agency(JAXA) ,3-1-1 Yoshino-dai, Chuo-ku, Sagamihara, Kanagawa 252-5210*

[8]*Department of Earth and Space Science, Osaka University, 1-1 Machikaneyama, Toyonaka, Osaka 560-0043*

[9]*ISS Science Project Office, Institute of Space and Astronautical Science (ISAS), Japan Aerospace Exploration Agency (JAXA), 2-1-1 Sengen, Tsukuba, Ibaraki 305-8505*

[10]*Department of Physics, Chuo University, 1-13-27 Kasuga, Bunkyo-ku, Tokyo 112-8551*

[11]*School of Dentistry at Matsudo, Nihon University, 2-870-1 Sakaecho-nishi, Matsudo, Chiba 101-8308*

[12]*Department of Physics, Nihon University, 1-8-14 Kanda-Surugadai, Chiyoda-ku, Tokyo 101-8308*

[13]*Department of Applied Physics, University of Miyazaki, 1-1 Gakuen Kibanadai-nishi, Miyazaki, Miyazaki 889-2192*

(Received ; accepted)

Abstract

The monitor of all-sky X-ray image (MAXI) Gas Slit Camera (GSC) on the International Space Station (ISS) detected a gamma-ray burst (GRB) on 2009, September 26, GRB 090926B. This GRB had extremely hard spectra in the X-ray energy range. Joint spectral fitting with the Gamma-ray Burst Monitor on the Fermi Gamma-ray Space Telescope shows that this burst has peculiarly narrow spectral energy distribution and is represented by Comptonized blackbody model. This spectrum can be interpreted as photospheric emission from the low baryon-load GRB fireball. Calculating the parameter of fireball, we found the size of the base of the flow $r_0 = (4.3 \pm 0.9) \times 10^9 Y'^{-3/2}$ cm and Lorentz factor of the plasma $\Gamma = (110 \pm 10) Y'^{1/4}$, where Y' is a ratio between the total fireball energy and the energy in the blackbody component of the gamma-ray emission. This r_0 is factor of a few larger, and the Lorentz factor of 110 is smaller by also factor of a few than other bursts that have blackbody components in the spectra.

Key words: gamma rays: bursts — methods: data analysis

1. Introduction

A discovery of the afterglows of gamma-ray bursts (GRBs) made it clear that GRBs are at cosmological distance and emit enormous energy. The spectra of GRB prompt emission have been expressed empirically with a smoothly broken power-law model ("Band Function") (Band et al., 1993). In order to explain the huge energy and non-thermal spectral shape, models of synchrotron emission from shock-accelerated electrons in the relativistic outflow (e.g. Rees & Meszaros, 1994) are suggested. However, sometimes the low-energy component is very hard and the power-law photon index α [1] becomes greater than the theoretical limit of 2/3 (Preece et al., 2002). This observational fact has been explained in many ways such as non-thermal (e.g. Medvedev et al., 2009; Lazzati & Begelman, 2010, and references therein) and thermal (e.g. Mészáros & Rees, 2000; Ryde, 2004; Beloborodov, 2010a) models, but reasons for such hard spectra have not been understood clearly. For example, Ghirlanda et al. (2003) suggest that some thermal models are consistent with observed spectral characteristics of several GRBs

[1] We use the photon index α in the context of E^α, where E is the energy, throughout this paper.

with extremely hard spectra. On the other hand, Sato et al. (2005) remark that "jitter" radiation (e.g. Epstein & Petrosian, 1973; Medvedev, 2000) is one of possible mechanisms of reproducing spectral indices $\alpha > -2/3$.

A GRB was triggered by Swift/BAT and Fermi/GBM at 21:55 on 2009 September 26. The quick results of this burst, GRB 090926B, are reported to GCN by the Swift team (Grupe et al., 2009) and the Fermi team (Briggs, 2009). Both of them conclude that the burst has a hard spectrum, whose photon index is $\alpha > -2/3$, above the critical value of synchrotron shock models, so-called "line of death". GRB 090926B was also observed with MAXI/GSC. MAXI/GSC can examine a low energy portion of the spectra of GRBs below 10 keV, while Swift/BAT or Fermi/GBM observes $\gtrsim$ 10 keV. The observational results below 10 keV may give even more severe constraints to interpretation of the spectra. In this paper, we report the observational results obtained with MAXI/GSC on GRB 090926B, and discuss their interpretation.

2. MAXI Observations and Data Analysis

2.1. Observations and Data reduction

Monitor of All-sky X-ray Image (MAXI) is a mission mounted on the International Space Station (ISS) (Matsuoka et al., 2009). The cameras of MAXI scan X-ray sources as the ISS rotates around the Earth. MAXI has two scientific instruments: the Gas Slit Camera (GSC; Mihara et al., 2011) and the Solid-state Slit Camera (SSC; Tomida et al., 2011). Since GRB 090926B was out of the SSC field of view, only the data of the GSC were available for the burst.

The GSC consists of twelve one-dimensional position sensitive proportional counters sensitive to 2–30 keV photons. Six GSC counters constitute an instantaneous field of view (FOV) of $3^\circ \times 160^\circ$ pointing toward the ISS motion (GSC-H), and the other six counters another FOV pointing to the zenith (GSC-Z). GSC-H and GSC-Z work together and covers 85% of the whole sky every ISS orbit. The transit time of a camera for a source is about 40–150 s, depending on the incident angle to the camera (See Sugizaki et al., 2011, for details).

GRB 090926B, the second GRB detected with MAXI, was observed with three cameras of the GSC: camera 0, 1, and 7. Total effective area for these three cameras is about 14 cm^2 at maximum[2]. Figure 1 is an image of GRB 090926B observed with the GSC. The GSC scanned the field from the right to the left in the image. The position localized by the GSC is reported to GCN by Morii et al. (2009) with an error circle of a radius of about 1 degree, which is shown in Figure 1. The position of the X-ray afterglow observed by Swift/XRT is pointed with the "X" mark in the same figure. The bright region of the image is clearly shifted toward the left relative to the XRT position. This is mostly because the intensity has changed during the scan. For a steady source, a point spread function must be symmetric on the source. In the case of GRB 090926B, the burst started when the source came across the FOV by 1/4, then brightened after the source passed the center of the FOV.

We also look into the data of other transits $\sim$ 5500 s before and after the burst. We cannot find any emission down to the flux limit of about 3×10^{-10} erg cm^{-2} s^{-1} (3σ) in the 4–10 keV band for either scan. According to the swift observation of the X-ray afterglow (Grupe et al., 2009), the energy flux at the time of the earliest MAXI scan after the burst was 7×10^{-12} erg cm^{-2} s^{-1} (0.3–10 keV), which was below the MAXI's detection limit.

For the light curve and spectral analyses, we use X-ray event data with processing version 0.3 provided by the MAXI team. This data set has time resolution of $\leq$ 1 ms and 1200 PI channel (1 PI = 0.05 keV). In addition to the GSC data, we use Fermi/GBM archival data[3], in order to compensate the limited energy range of the GSC. We use *XSELECT* ver. 2.4a and *XSPEC* ver. 12.5.0ac for the data selection and spectral analyses, respectively.

2.2. Light curves

Figure 2 shows the light curves of GRB 090926B with MAXI/GSC and Fermi/GBM. The count rate of MAXI/GSC is corrected for the effective area, which is shown in the bottom panel of the figure. Although MAXI/GSC covered only the first 30 s of the prompt emission, the burst actually lasted for more than 50 s; Grupe et al. (2009) (Swift) and Briggs (2009) (Fermi) report the burst duration of $T_{90} = 109.7 \pm 11.3$ s and $T_{90} = 81 \pm 13$ s, respectively. As seen in Figure 2, it shows a relatively hard spectrum in the first 15 s. By contrast, the spectrum becomes relatively soft in the following part of the burst.

2.3. Spectral analysis

The results of the time averaged spectra of the burst observed with Swift and Fermi are reported to GCN by Grupe et al. (2009) and Briggs (2009), respectively. Both teams mention that the spectrum can be fit with a cutoff power law model. Briggs (2009) integrate the spectrum in the first 48.6 s, and find the peak energy in the EF_E spectrum (where F_E is the energy flux at energy E) of $E_{peak} = 91 \pm 2$ keV and α = -0.13 $\pm$ 0.06. Grupe et al. (2009) adopt a longer (154.8 s) integration time and find E_{peak} = 78.3 $\pm$ 7.0 keV and α = -0.52 $\pm$ 0.24. These photon indices are remarkably large, well above the line of death.

Since these results are derived from analyses above $\sim$ 10 keV, we examine whether or not this power-law is extended to energies below 10 keV, using the MAXI/GSC data. First, we extract a time averaged spectrum from $T_0-1.5$ to $T_0+28.5$ s, where T_0 is the trigger time of Fermi (2009 September 26, 21:55:28). To reduce the statistical uncertainty of the photon index due to the limited energy range of the GSC, we then simultaneously fit the spectra of the GSC together with that of Fermi/GBM. We test

[2] The effective area of MAXI/GSC to a source changes during the $\sim$ 40 s transit time as a triangular curve.

[3] http://fermi.gsfc.nasa.gov/ssc/data/access/gbm/

both a cutoff power law model and the empirical "GRB model" (Band et al., 1993), which has 4 free parameters, a photon index in the lower energy band α, that in the higher band β, a peak energy E_{peak}, and a normalization. The results are summarized in Table 1.

To study the spectral evolution during the burst, we divide the spectra into three time intervals. As noticed from Figure 2, there are two distinct peaks in the light curve in the 100–350 keV band at T_0+6.5 s and T_0+17.5 s. Accordingly, the first, second, and last intervals are defined as between $T_0-1.5$–T_0+6.5 s (before the first peak), $T_0-6.5$–T_0+17.5 s (in-between the two peaks), and $T_0-17.5$–T_0+28.5 s (after the second peak), respectively. The fitting results of the time resolved spectra are also summarized in Table 1.

3. Discussions

The earlier reports on the spectral analyses of GRB 090926B from the Swift and Fermi teams suggested very flat spectra represented by a cut-off power law with a photon index of -0.52 ± 0.24 and -0.13 ± 0.06 (Grupe et al., 2009; Briggs, 2009), and E_{peak} of 78.3±7.0 keV and 91±2 keV, respectively. We confirm these results from the combined spectra of MAXI/GSC and Fermi/GBM. Using the time averaged spectrum, we obtain the best fit cut-off power-law model with $\alpha = 0.44 \pm 0.14$ and E_{peak} of 97 ± 7 keV. The discrepancy between our result and that by the Fermi team mainly comes from the difference of the time interval, rather than the energy range, used for the spectral analyses; while Briggs (2009) utilize the first 48.6 s data, we analyze only the first 30 s after the burst. Indeed, from the analysis of GBM data alone, we had the result consistent with the result of joint fit analysis, when we limit the time range to first 30 s. When the "GRB model" is adopted, we obtain the index $\alpha = 0.65 \pm 0.20$ and $E_{peak} = 85 \pm 9$ keV. In either model, the obtained α value exceeds the line of death. Moreover, the spectral parameters are peculiar among GRBs. The E_{peak} and α values are plotted in the scatter plot in Figure 4 together with those of the BATSE sample taken from Kaneko et al. (2006). The point of GRB 090926B is apart from the "main sequence", and has both larger α and smaller E_{peak} compared with the majority of GRBs.

Let us consider the mechanisms to produce such a high α spectrum. First, we investigate the possibility that the photons are heavily absorbed somewhere between the source and the earth. To investigate this possibility, we fit the time averaged spectrum with an absorbed "GRB model", where the absorber is assumed to be located at redshift of $z = 1.24$ (Fynbo et al., 2009). We obtain the best-fit absorption column density $N_{\rm H}$ consistent with zero[4] and $\alpha = 0.71$. Since the column density is often coupled with the power-law photon index, the confidence contours in the α-$N_{\rm H}$ space are drawn in Figure 5. From this figure, a lower limit of α is found to be 0.42 (90% confidence), and thus we conclude that the large photon index cannot be explained by an interstellar absorption.

Then we have to consider the possibility that the burst has intrinsically large α. Ghirlanda et al. (2003) discussed various models reproducing extremely hard spectra, including the bursts with the low-energy photon indices α larger than 1. Similar discussions are presented in Sato et al. (2005) about GRB 020813, which had the flattest spectrum among the bursts detected by HETE-2. They studied the case of synchrotron self absorption and synchrotron self Compton as well. We can calculate the source radius and the electron number density, from the redshift z=1.24 (Fynbo et al., 2009), $E_{peak} = 85$ keV, and total energy of the burst $E_{tot} = 4.3 \times 10^{52}$ ergs, following Sato et al. (2005).

For the case of synchrotron self absorption, we obtain the source radius $r = 5.9 \times 10^{13}$ cm, minimum Lorentz factor of relativistic electrons $\Gamma_m = 400$, electron number density $n = 10^{13}$ cm^{-3}, and magnetic field strength $B = 2.9 \times 10^5$ gauss. As mentioned in Sato et al. (2005), the peak flux calculated from the above parameters is inconsistent with the observed value unless we assume unusual physical conditions of the source. For the case of synchrotron self Compton, we have $r = 3.1 \times 10^{16}$ cm, $\Gamma_m = 240$, $n = 1.2 \times 10^5$ cm^{-3}, and $B = 24$ gauss. These results are quite similar to the results of GRB 020813, and then synchrotron self Compton model cannot be appropriate because of the large radius. Interestingly, the redshift of GRB 020813 $z = 1.25$ is close to that of GRB 090926B ($z = 1.24$) presumably. The other parameters also agree within an order of magnitude. Therefore, the discussion for GRB 020813 is also appropriate for GRB 090926B.

Jitter radiation, which is emitted by ultra-relativistic electrons in highly nonuniform, small-scale magnetic fields, is studied as one of the mechanisms responsible for such a hard low-energy index (e.g. Medvedev et al., 2009, and references therein). Reynolds et al. (2010) studied the observable spectral shape of the jitter radiation from various conditions of magnetic field. According to their work, despite the comprehensive search of the enormous parameter space, it is not possible to find the condition to generate an index α larger than 0. On the other hand, we found from the fitting results that the probability of $\alpha \leq 0$ is order of 10^{-6}. Therefore, the spectrum of GRB 090926B may not be produced by jitter radiation.

Another possibility is that the spectrum is produced by thermal radiation. Thermal components in the spectra of GRB prompt emission were claimed to appear for several GRBs (Ryde et al., 2010, and references therein). Some bursts showed spectra reproduced by blackbody + power-law components, and sometimes a power-law component was not necessary to represent the observed spectra (Ryde et al., 2006). Indeed, its spectrum has a positive low-energy index and shows a narrow energy distribution. Figure 6 shows the spectral energy distribution of this burst. Compared with a typical GRB (plotted with thin solid line), this burst has lower E_{peak} and a steeper rising part, which is rather close to the Rayleigh-Jeans part of a blackbody spectrum (plotted with thin dotted line). The

[4] The Galactic value of the absorption column density toward the burst direction is 1.91×10^{20} cm^{-2}.

thermal components of GRBs could be considered to be a contribution of the photosphere of GRB fireball. Mészáros & Rees (2000) studied various cases of GRB spectra based on the internal shock model consisting of a photospheric component and Comptonized element by the pair plasma.

Following Paczynski (1986), the observable radius and temperature of the blackbody radiation from the photosphere is constant during the acceleration of the flow. Therefore, if we can estimate the parameters of the blackbody, they are the parameters of the innermost part of the burst. In order to derive the photospheric radius and temperature, we test a model of simple blackbody radiation first. However, this model does not give a good fit owing to the tail-like component in the high energy part. This fact can be naturally interpreted as a temporal or a spatial superposition of the multiple temperature rather than fully adiabatic and uniform photosphere.

Then we adopted a model of Comptonized blackbody model (Nishimura et al., 1986) for the purpose of fitting both the blackbody-like component and high energy tail. The results of this fit are shown in the bottom part of Table 1.

Pe'er et al. (2007) introduced the method to calculate the parameters of photosphere from the observed spectral parameters, under the condition that the Lorentz factor of the plasma Γ is directly proportional to the radius of the fireball. There is a key parameter that indicates the ratio of the observed flux and emitted flux

$$\mathcal{R} \equiv \left(\frac{F_{\mathrm{BB}}^{ob}}{\sigma T^{ob\,4}} \right)^{1/2}, \tag{1}$$

where σ is Stefan-Boltzmann constant, F_{BB}^{ob} is the observed flux of the blackbody component, and T^{ob} is the observed blackbody temperature. We used the equations

$$\Gamma = \left[(1.06)(1+z)^2 d_{\mathrm{L}} \frac{Y F^{ob} \sigma_{\mathrm{T}}}{2 m_{\mathrm{p}} c^3 \mathcal{R}} \right]^{1/4}, \tag{2}$$

$$r_0 = \frac{4^{3/2}}{(1.48)^6 (1.06)^4} \frac{d_{\mathrm{L}}}{(1+z)^2} \left(\frac{F_{\mathrm{BB}}^{ob}}{Y F^{ob}} \right)^{2/3} \mathcal{R}, \tag{3}$$

where z, d_{L}, σ_{T}, m_{p}, and c are the redshift, luminosity distance to the source, Thomson cross section, proton mass, and speed of light, respectively. The parameter Y is a ratio between the total fireball energy and the energy emitted in gamma-rays. The ratio of the total observed flux to the blackbody component F^{ob}/F_{BB}^{ob} depends on the energy range of integration, particularly on the upper bound, because Comptonized component dominates in higher energy part. For example, $F^{ob}/F_{BB}^{ob} \sim 1.0$ for the upper bound of 800 keV and 1.2 for 1200 keV. Consequently we introduce the renormalized parameter $Y' = Y F^{ob}/F_{BB}^{ob}$ instead of Y. The luminosity distance corresponding to the measured redshift $z = 1.24$ is $d_{\mathrm{L}} = 2.68 \times 10^{28}$ cm under the standard condition of $H_0 = 71$ km s^{-1} Mpc^{-1}, $\Omega_\Lambda = 0.73$, and $\Omega_{\mathrm{M}} = 0.27$. Using the temperature of the blackbody radiation $kT = 17.2$ keV and its observed flux $F_{\mathrm{BB}}^{ob} = 3.0 \times 10^{-7}$ erg cm^{-2} s^{-1}, we find the Lorentz factor of the plasma $\Gamma = (110 \pm 10)\, Y'^{1/4}$, and the physical size at the base of the flow $r_0 = (4.3 \pm 0.9) \times 10^9\, Y'^{-3/2}$ cm. These values are factor of a few different from the case of GRB 970828, GRB 990510 (Pe'er et al., 2007), or GRB 090902B (Ryde et al., 2010).

According to Beloborodov (2010b), the observed photospheric spectrum is blackbody if the outflow energy is dominated by radiation rather than baryon up to the photospheric radius. In other words, the fireball remained optically thick when the initial acceleration was saturated. This situation occurs in the case of low baryon load. The spectrum of GRB 090926B may be one of the extreme example of the low baryon-load fireball.

4. Conclusion

MAXI GSC observed the first 30 s of GRB 090926B prompt emission. From the data of the scans before and after the burst, we could not find any signal of emissions with the flux limit of about 3 $\times 10^{-10}$ erg cm^{-2} s^{-1} (4–10 keV) for each scan. The joint spectral analysis with Fermi GBM reveals that the spectrum of GRB 090926B shows a peculiar narrow shape. The spectral index α of time averaged spectrum is positive. The E_{peak} of the burst is low relative to other bursts with such a hard spectral indices. This hard spectral index cannot be realized by interstellar absorption, synchrotron self absorption, synchrotron self Compton, nor jitter radiation. We find that the spectrum can be fit well by Comptonized blackbody model. The blackbody radiation can be interpreted as a photospheric emission of the GRB fireball. Following the model by Pe'er et al. (2007), we obtain the size of the base of the flow $r_0 = (4.3 \pm 0.9) \times 10^9 Y'^{-3/2}$ cm and Lorentz factor of the plasma $\Gamma = (110 \pm 10)\, Y'^{1/4}$. According to Beloborodov (2010b), the observed photospheric spectrum is blackbody if the outflow energy is dominated by radiation rather than baryon up to the photospheric radius. Therefore, the spectrum of GRB 090926B may be the example of the low baryon-load fireball.

This research was partially supported by the Ministry of Education, Culture, Sports, Science and Technology (MEXT), Grant-in-Aid No.19047001, 20041008, 20244015, 20540230, 20540237, 21340043, 21740140, 22740120, and Global-COE from MEXT "The Next Generation of Physics, Spun from Universality and Emergence" and "Nanoscience and Quantum Physics".

References

Band, D., et al. 1993, ApJ, 413, 281
Beloborodov, A. M. 2010a, MNRAS, 407, 1033
Beloborodov, A. M. 2010b, arXiv:1011.6005
Briggs, M. S. 2009, GRB Coordinates Network, 9957, 1
Epstein, R. I., & Petrosian, V. 1973, ApJ, 183, 611
Fynbo, J. P. U., et al. 2009, GRB Coordinates Network, 9947, 1
Ghirlanda, G., et al. 2003, A&A, 406, 879
Grupe, D., et al. 2009, GCN Report, 246, 1
Kaneko, Y., et al. 2006, ApJS, 166, 298

Lazzati, D., & Begelman, M. C. 2010, ApJ, 725, 1137
Matsuoka, M., et al. 2009, PASJ, 61, 999
Medvedev, M. V. 2000, ApJ, 540, 704
Medvedev, M. V., Pothapragada, S. S., & Reynolds, S. J. 2009, ApJL, 702, L91
Mészáros, P., & Rees, M. J. 2000, ApJ, 530, 292
Mihara, T., et al. 2011, PASJ, accepted, arXiv:1103.4224
Morii, M., et al. 2009, GRB Coordinates Network, 9943, 1
Nishimura, J., Mitsuda, K., & Itoh, M. 1986, PASJ, 38, 819
Paczynski, B. 1986, ApJL, 308, L43
Pe'er, A., Ryde, F., Wijers, R. A. M. J., Mészáros, P., & Rees, M. J. 2007, ApJL, 664, L1
Preece, R. D., et al. 2002, ApJ, 581, 1248
Rees, M. J., & Meszaros, P. 1994, ApJL, 430, L93
Reynolds, S. J., Pothapragada, S., & Medvedev, M. V. 2010, ApJ, 713, 764
Ryde, F. 2004, ApJ, 614, 827
Ryde, F., et al. 2006, ApJ, 652, 1400
Ryde, F., et al. 2010, ApJL, 709, L172
Sato, R., et al. 2005, PASJ, 57, 1031
Sugizaki, M., et al. 2011, PASJ, accepted, arXiv:1102.0891
Tomida, H., et al. 2011, PASJ, 63, 397

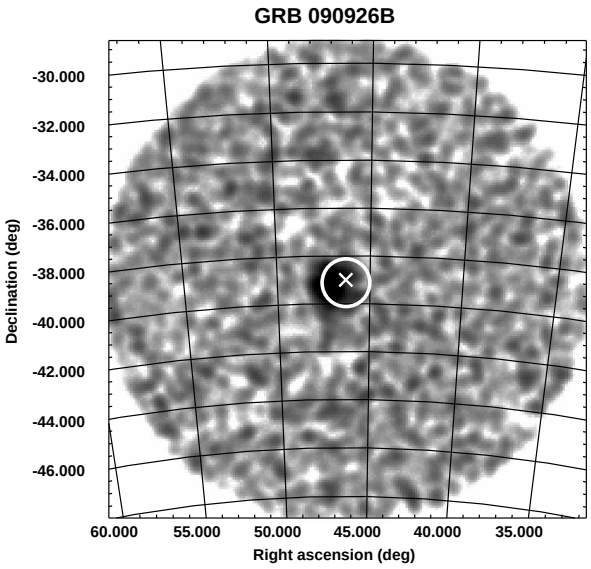

Fig. 1. MAXI GSC image of GRB 090926B. The MAXI error circle reported to GCN (Morii et al., 2009) is shown. The "X" mark denotes the position of the GRB derived by Swift XRT (Grupe et al., 2009).

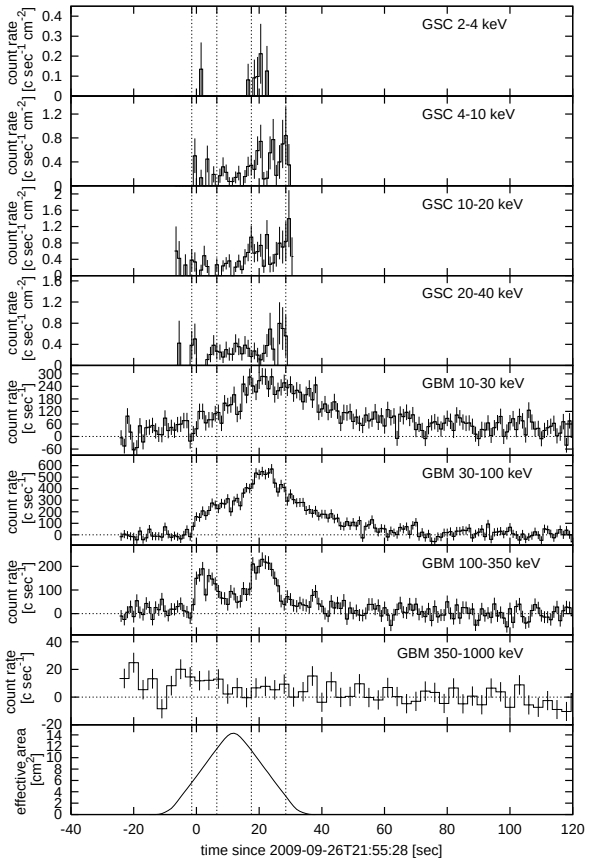

Fig. 2. The light curves of GRB 090926B observed with MAXI/GSC and Fermi/GBM. The light curves of GSC are corrected for the effective area. The change of the effective area is shown in the bottom panel. The vertical dashed lines indicate the borders of the time intervals for spectral analyses.

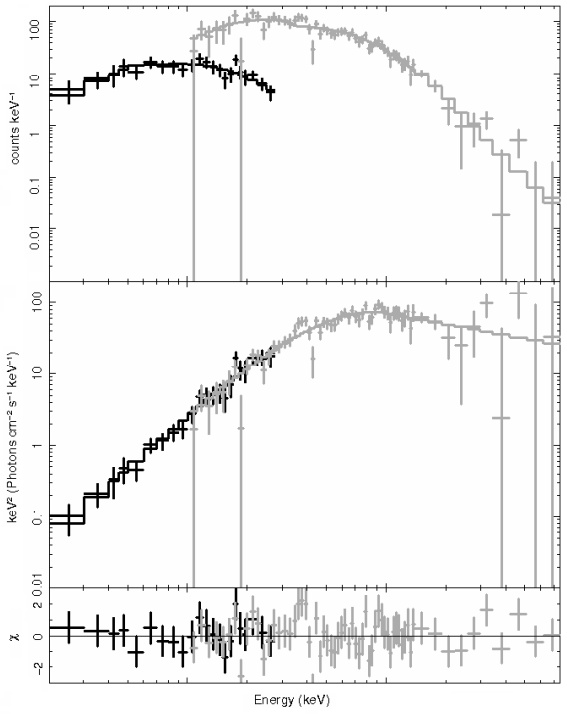

Fig. 3. Time average spectrum of GRB 090926B fitted with the "GRB model". The top panel shows the data and the folded model, and the middle panel shows the unfolded EF_E spectrum. The residuals are plotted in the bottom panel. The data sets of the GSC and GBM are plotted in black and gray, respectively.

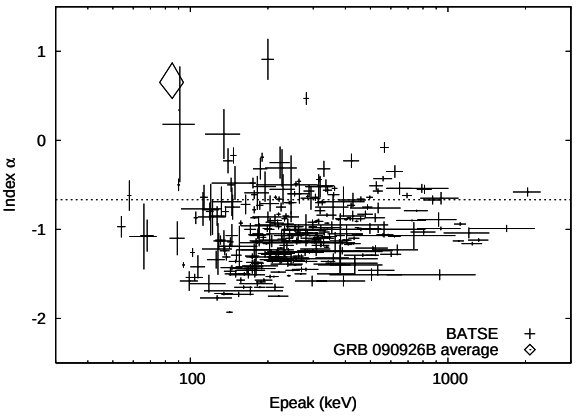

Fig. 4. Scatter plot on the E_{peak}-α plane. The open diamond represents the time averaged spectrum of GRB 090926B. The BATSE sample from Kaneko et al. (2006) is plotted with crosses.

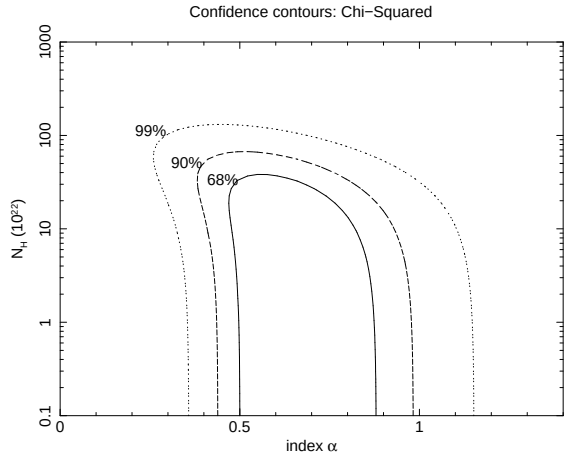

Fig. 5. Confidence contours of α-$N_{\rm H}$ space for the time averaged spectrum. The confidence levels of 68%, 90%, and 99% are shown.

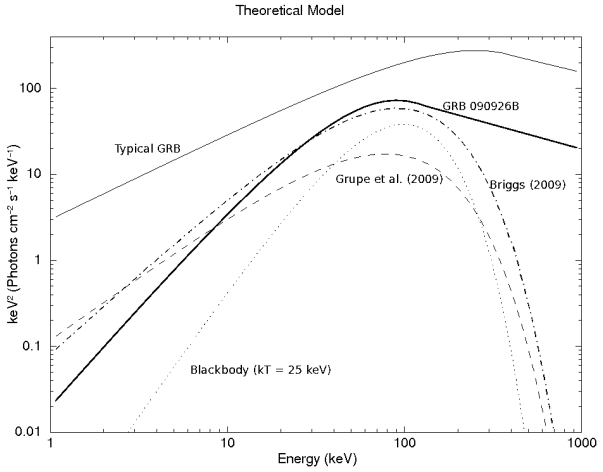

Fig. 6. The best fit model of the time averaged spectrum is plotted with thick solid line in the EF_E space. A typical GRB spectrum with $\alpha = -1$, $\beta = -2.5$, and $E_{peak} = 250$ keV is shown with thin solid line. A sample of blackbody spectrum with kT = 25 keV is shown with thin dotted line. The spectral models reported to GCN by the Swift team (Grupe et al., 2009) and the Fermi team (Briggs, 2009) are plotted with dashed and dash-dotted lines respectively. Note that they represent the averaged spectra of the different time interval in the burst (see text).

Table 1. Spectral parameters of GRB 090926B

	time interval			
component	T_0−1.5 – T_0+28.5	T_0−1.5 – T_0−6.5	T_0−6.5 – T_0+17.5	T_0+17.5 – T_0+28.5
cut-off power law				
χ^2(DoF)	93.26 (83)	20.56 (32) *	65.41 (67)	100.17 (81)
Index α (E^{α})	$0.44^{+0.14}_{-0.13}$	$0.43^{+0.47}_{-0.33}$	$0.76^{+0.31}_{-0.26}$	$0.24^{+0.20}_{-0.17}$
E_{peak} (keV)	97^{+7}_{-6}	142^{+30}_{-21}	76^{+9}_{-7}	96^{+8}_{-7}
Normalization †	$4.3^{+0.4}_{-0.3}$	$1.6^{+0.4}_{-0.5}$	$4.6^{+0.8}_{-0.7}$	$6.9^{+0.8}_{-0.8}$
GRB model				
χ^2(DoF)	83.13 (82) *	20.56 (31)	61.90 (66)	94.65 (80) *
Index α (E^{α})	$0.65^{+0.22}_{-0.18}$	$0.42^{+0.31}_{-0.31}$	$1.07^{+0.61}_{-0.41}$	$0.52^{+0.34}_{-0.25}$
Index β (E^{β})	$-2.51^{+0.29}_{-0.49}$	-9.37 ‡	$-2.67^{+0.46}_{-1.71}$	$-2.53^{+0.32}_{-0.71}$
E_{peak} (keV)	85^{+9}_{-9}	143^{+29}_{-16}	67^{+12}_{-11}	83^{+11}_{-10}
Normalization †	$4.5^{+0.6}_{-0.5}$	$1.7^{+0.5}_{-0.5}$	$5.2^{+2.0}_{-1.1}$	$7.2^{+1.1}_{-0.9}$
Comptonized blackbody §				
χ^2(DoF)	88.45 (83)	22.31 (32)	61.20 (67) *	100.86 (81)
temperature kT (keV)	$17.2^{+1.1}_{-1.0}$	$29.0^{+5.3}_{-4.5}$	$15.3^{+1.6}_{-1.5}$	$16.5^{+1.4}_{-1.3}$
Normalization ‖ (10^{10} cm)	$4.9^{+0.7}_{-0.6}$	$1.6^{+0.8}_{-0.6}$	$5.0^{+1.2}_{-1.0}$	$6.1^{+1.2}_{-1.0}$
optical depth τ	$0.9^{+0.2}_{-0.2}$	$0.5^{+0.6}_{-0.5}$	$0.7^{+0.3}_{-0.3}$	$0.8^{+0.2}_{-0.2}$

* Best fit model to the spectrum.
† Normalizations are in the unit of 10^{-2} photons cm^{-2} s^{-1} keV^{-1} at 15 keV.
‡ Errors are not available.
§ The electron temperature is fixed to 50 keV.
‖ Normalizations are given as a radius of blackbody, on the assumption of redshift z=1.24.